IEEE TRANSACTIONS ON MAGNETICS, VOL. 51, NO. 11, NOVEMBER 2015

DOI: 10.1109/TMAG.2015.2436924,

Effect of Superparamagnetic Fe_3O_4 Nanoparticles on Schottky Barriers of Graphene

Junran Zhang,[1] Zhenyao Wu,[1] Minhao Zhang,[1] Wei Niu,[1] Ming Gao,[1] Ying Zhou,[1] Wenqing Liu[2], Xuefeng Wang,[1,a)] Rong Zhang,[1] and Yongbing Xu[1,2,a)]

[1]Jiangsu Provincial Key Laboratory of Advanced Photonic and Electronic Materials, Collaborative Innovation Center of Advanced Microstructures, School of Electronic Science and Engineering, Nanjing University, Nanjing 210093, China

[2]York-Nanjing Joint Centre (YNJC) for spintronics and nano engineering, Department of Electronics, The University of York, YO10 3DD, United Kingdom

Abstract

We demonstrated the effect of superparamagnetic Fe_3O_4 nanoparticles on Schottky barriers of graphene, in which the Fe_3O_4 nanoparticles were fabricated by a hydrothermal method and the single-layer graphene sheets were mechanically exfoliated from Kish graphite. The Fe_3O_4 nanoparticles were superparamagnetic with the saturation magnetic moment of about 32 emu/g at room temperature. We have found that the Fe_3O_4 nanoparticles decorated on the graphene surface can dramatically modify the Schottky barriers of the whole devices possibly due to the magnetic stray field from the Fe_3O_4 nanoparticles in proximity to the graphene. . The Schottky barrier could be tuned by the quantity of Fe_3O_4 nanoparticles.

Keywords

Fe_3O_4 nanoparticles, graphene, Superparamagnetism, Schottky barrier

[a)] Authors to whom correspondence should be addressed. E-mail addresses: xfwang@nju.edu.cn and ybxu@nju.edu.cn.

Half-metal magnetite (Fe_3O_4) is a widely studied material as it presents unique properties such as the theoretically 100 % spin polarization at the Fermi level [1], the metal-insulator transition (Verwey transition) at 120 K [2, 3], the ferromagnetic nature with Curie temperature of 858 K, the largely unquenched orbital moment [4], and the multiferroicity at low temperatures [5]. The merits of magnetite offer unique opportunities for both material science and engineering [6]. At room temperature, Fe_3O_4 is a conductor (conductivity is about 2.5×10^4 $(\Omega\cdot cm)^{-1}$) [7], and its conductivity decreases with decreasing temperature. The good conductivity of magnetic Fe_3O_4 thin film above Verwey transition temperature will interfere the electrical research of heterostructures with other conductor. However, the uniformly dispersed superparamagnetic Fe_3O_4 nanoparticles are insulating because of the interspace among Fe_3O_4 nanoparticles. For every individual Fe_3O_4 nanoparticles, it has a net magnetic moment, which will contribute to a local stray field, in spite of total superparamagnetism for large quantity nanoparticles [8]. Accordingly, Fe_3O_4 nanoparticles have uniquely superiority in studying the electrical and magnetic transport properties for Fe_3O_4/graphene composite structure.

Graphene is a single-layer of carbon atoms arranged in two-dimensional hexagonal honeycomb lattice, and has attracted lots of interests due to its unique chiral Dirac electronic spectrum [9, 10]. A crucial challenge for graphene-based spintronics is to develop magnetic order, or even long-range ferromagnetic order in graphene [11]. Graphene possesses large phase coherence length of up to ~8 μm for spin injection [12, 13], holding great potential for spintronic applications.

The surface decoration of graphene offers huge opportunities because graphene is a fully open system [14, 15]. Functional defects, p/n type doping, and additional spin- orbit interactions can be introduced when atoms are intimately absorbed from an external source [16-25]. One has even considered to induce topologically nontrivial gaps inside the Dirac cone. It has been suggested that magnetic attachments that break the time reversal symmetry of graphene can induce pseudospin organization, which would result in topologically nontrivial states [22, 26]. Adatom adsorptions (In, Tl, and Pb) are believed to generate a gap

within the Dirac cone, thereby introducing the quantum spin Hall effect in graphene sheets [16]. Zhang et al. theoretically calculated the Ir and W (5d) atom attachments can mediate a quantum anomalous Hall state induced by large spin-orbit interaction of the 5d metals [27]. Hong et al. has experimentally shown that spin-flip scattering can be introduced by fluorine doping [21]. Han et al. achieved tunneling spin injection from Co into single-layer graphene and observed a nonlocal magnetoresistance of 130 Ω at room temperature, which is the largest value at that time [20]. Qin et al. confirmed that Pd deposition on graphene can enhance quantum coherence [28]. Furthermore, magnetic decoration of graphene is more fascinating because of proximity-induced ferromagnetism in graphene and thus one can obtain the ferromagnetic graphene without sacrificing its excellent transport properties [29, 30]. spintronic systems for the study of novel electrical and magnetic transport properties. However, up to now most studies have focused on enhancing lithium storage rate [31]. The effect of electrical and magnetic transport properties of graphene by attachment/decoration of Fe_3O_4 nanoparticles has still remained unknown. In this work, we report the fabrication and characterization of Fe_3O_4 nanoparticles and graphene composite structures. The tunable Schottky barriers of graphene by Fe_3O_4 nanoparticles were observed for the first time.

II. EXPERIMENT

Alcohol-soluble Fe_3O_4 nanoparticles were synthesized by hydrothermal method. In brief, $FeCl_3 \cdot 6H_2O$ (0.8109 g) and $NaHCO_3$ (0.756 g) were dissolved in deionized water (30 ml) with the aid of magnetic stirring. Meanwhile, L-ascorbic acid (0.088 g) was separately dissolved in deionized water (10 ml) by stirring. After 30 min, two solutions were mixed and the stirring continued for another 20 min. Finally, the solution was transferred into a 125 ml Teflon-lined stainless-steel autoclave and heated at around 150 oC for 6 h in a furnace. The as-obtained nanoparticles were collected by centrifuge and washed by alcohol and de-ionized water several times. Finally, the particles were dispersed in alcohol solution in view of its effumability.

Single-layer graphene sheets were exfoliated from Kish graphite flakes and on a silicon wafer with 300-nm-thick silicon dioxide layer. Devices were fabricated using a

standard electron-beam lithography and Au (60 nm thickness) electron-beam evaporation. There are 4 device samples, denoted as S1, S2, S3 and S4. In order to accelerate the evaporation of alcohol, before measuring the current-voltage (I-V) curves, the devices dripping with alcohol or alcohol-soluble Fe_3O_4 nanoparticles were baking for 5 min at 50 oC.

The morphology and magnetic properties of Fe_3O_4 nanoparticles were characterized by a scanning electron microscope (SEM, JEOL, JSM-7100F), transmission electron microscope (TEM, JEM-200CX), atomic force microscopy (AFM) and vibrating sample magnetometer (VSM), respectively. Graphene sheets were confirmed as single-layer by a laser Raman spectrometer (JY HR800). Electrical curves were measured by Keithley 4200-SCS electrometer.

III. RESULTS AND DISCUSSIONS

Figure 1 shows the magnetic hysteresis loop of Fe_3O_4 nanoparticles measured by VSM (black solid rectangle), indicating the superparamagnetism of the Fe_3O_4 nanoparticles whose saturation magnetic moment is about 32 emu/g. For superparamagnetic particles, the true magnetic moment at a particular temperature can be calculated using the Langevin function [32] :

$$M = M_S\left(\coth\left(\frac{\mu_H}{k_bT}\right) - \frac{k_bT}{\mu_H}\right) \qquad (1)$$

Where μ (= $M_S\pi D^3/6$) is the true magnetic moment of each particle, k_b is the Boltzmann constant, T is the absolute temperature, D is the mean diameter of each particles and M_S is the saturation magnetization. The red solid line in Fig. 1 shows the best fit for the Langevin function in Eq. (1). From this data fitting, the mean diameter of each particles is 12.32 nm, which is corresponding to the value from SEM and TEM.

Left top and bottom insets are SEM and TEM images of Fe_3O_4 nanoparticles, respectively, indicating granular and uniform morphology of the Fe_3O_4 nanoparticles. SEM and TEM results also show that the diameter of Fe_3O_4 nanoparticles is about 10 nm with a

standard deviation of 5nm based on estimation from 100 nanoparticles. Right bottom inset is photograph before and after the magnet attraction. It shows that Fe_3O_4 nanoparticles can be attracted by magnet after several minutes. Although the total magnetic moment of large quantity Fe_3O_4 nanoparticles is zero revealed by superparamagnetism in macroscopy, each individual Fe_3O_4 nanoparticle has magnetic moment because the particles can be attracted by magnet as shown in the right bottom inset of Fig. 1. Namely, it has no magnetic influence on graphene in macroscopy, but each individual Fe_3O_4 nanoparticle will be a magnetic source forming a stray field to graphene and then affecting the properties of graphene, as discussed below.

Raman scattering spectroscopy was performed to confirm that graphene is single layer as shown in Fig. 2. We can see both the characteristic G (~1580 cm^{-1}) and 2D (~2700 cm^{-1}) peaks of single-layer graphene. The 2D peak (full width at half maximum is 31.2 cm^{-1}) and 2D/G ratio indicate that the sample is a single-layer graphene sheet, D peak (~1350 cm^{-1}) associated with defects is not observed. Left inset is optical micrograph of single-layer graphene. The dashed lines show the edges of the single- layer graphene sheet. Only 2.3 % incident light is absorbed by single-layer graphene [33]. Thus, the contrast of graphene on silicon oxide wafer is not distinct. Appreciable contrast of the single-layer graphene with bottom adjacent triangular purple multi-layer graphene region was observed (see the left inset). Right inset shows an AFM image of the graphene sheet with Fe_3O_4 nanoparticles. The Fe_3O_4 nanoparticles appear to be granular and discrete. AFM image reveals that Fe_3O_4 nanoparticles are dispersed on the graphene surface with a very low coverage of less than 5 %.

The inset in Fig. 3(a) shows the photograph of the device (S1) fabricated by electron-beam lithography and Au electron-beam evaporation, in which the electrodes and channels are both 2 μm wide. The dashed lines show the edges of the single-layer graphene sheet. All of our devices were measured with two-probe method. There are two kinds of contact from our pure graphene measurement, namely, Ohmic contact and Schottky contact as shown in Fig. 3(a) and Fig. 3(b), respectively. Different contact type of pure graphene may

come from the process of devices fabrication.

From black rectangle solid and red circle solid straight line in Fig. 3(a), it can be seen that S1 (pure graphene) is Ohmic contact, and the resistance is about 1000 Ω. However, when we measured S1 of graphene with baking for 5 min at 50 oC after dripping 0.05 ml solution with alcohol-soluble Fe_3O_4 nanoparticles, it becomes Schottky contact, as shown in right bottom inset of Fig. 3 (a). In order to eliminate the influence of alcohol to the graphene, we measured the graphene with 0.05 ml alcohol without Fe_3O_4 nanoparticles (S2). Before measurement, we also baked the device for 5 min at 50 oC to accelerate the alcohol evaporation without damaging the device. The red circle solid straight line in Fig. 3(a) shows that it is still Ohmic contact and the resistance is about 857 Ω, which is slightly reduced possibly due to the extra conductivity contributed by residual alcohol.

Fig. 3(b) and inset of Fig. 3(b) show the *I–V* curves of S3 and S4. In which, Fig. 3(b) is the *I–V* curves of S3 (graphene decorated with different volume solutions of Fe_3O_4 nanoparticles). Inset of Fig. 3(b) is I-V curves of S4 measured at larger voltage. From the I-V curves, we can see that both devices show Schottky contact no matter pure graphene and graphene decorated with Fe_3O_4 nanoparticles. After decorated with Fe_3O_4 nanoparticles, the Schottky barrier becomes larger, and the Schottky barrier can be tuned by the quantity of Fe_3O_4 nanoparticles. In other words, the resistance of device decreases because of decoration of Fe_3O_4 nanoparticles.

Using the thermionic emission theory, our devices can be seen as Au/graphene/Au junction, the current densities in a metal/semiconductor/metal junction is written as [34]

$$J_{1(T)} = A^*T^2\exp\left(-\frac{q\Phi_{B1}}{k_BT}\right)\times\left[\exp\left(-\frac{qV_1}{k_BT}\right)-1\right] \quad (2)$$

$$J_{2(T)} = -A^*T^2\exp\left(-\frac{q\Phi_{B2}}{k_BT}\right)\times\left[\exp\left(-\frac{qV_2}{k_BT}\right)-1\right] \quad (3)$$

Where A* is the Richardson constant, Φ_{B1} and Φ_{B2} are the Schottky barrier heights and the other symbols have their usual meanings. Obviously the voltage saturates in both directions, but maybe at different values, just like the I-V curve in right bottom inset of Fig. 3(a). The

larger Φ_{B1} and Φ_{B2} reveal that Fe_3O_4 nanoparticles have some influence on metal/semiconductor/metal junctions.

Owing to the high spin polarization of Fe_3O_4, the carriers in graphene will be spin- polarized. Wang et al. reported that graphene has spin-polarized carriers coming from proximity with yttrium iron garnet [30]. And the magnetism of each individual Fe_3O_4 nanoparticles forms external stray field. In this case, Tang et al. proposed a model to simulate the situation of devices with spin-polarized carriers [34]. They treated carrier states as nondegenerate and its splitting produces spin-polarized electrons. The splitting of carrier bands can be of exchange or Zeeman type. So, a two-current model is applied to the analysis. The Δ_{ex} and $\mu_B B$ (μ_B denotes the Bohr magneton) are defined as the exchange energy and the Zeeman energy, respectively. When an external magnetic field B is applied, the carrier energy is Zeeman split: up-spin and down-spin electrons undergo energy shifts of $\pm\mu_B B$, respectively. Therefore, the conduction-band edges for the graphene are given by $E_{c\uparrow(\downarrow)} = E_c - (+)\Delta_{ex}/2 - (+)\mu_B B$, where E_c is treated as an average conduction-band edge. Based on the double thermionic emission model and considering the spin-split in the conduction band, the spin-dependent current density is given by [35]

$$J_{1(\uparrow(\downarrow))(T)} = \frac{1}{2}A^*T^2\exp\left(-\frac{q\Phi_{B1} - (+)\frac{\Delta_{ex}}{2} - (+)\mu_B B}{k_B T}\right) \times \left[\exp\left(-\frac{qV_1}{k_B T}\right) - 1\right]. \quad (4)$$

From Eq. (4), we can see that current density J decreases compared with Eq. (2) when there is an external field. This explain that the resistance of device decreases while adding the quantity of Fe_3O_4 nanoparticles solutions. With the same current density J, Schottky barrier height Φ increases with increasing external stray field B, when adding the quantity of Fe_3O_4 nanoparticles.

IV. CONCLUSION

We have demonstrated the influence of superparamagnetic Fe_3O_4 nanoparticles on Schottky barriers of graphene, in which the Fe_3O_4 nanoparticles were synthetized by a hydrothermal

method and the single-layer graphene sheets were mechanically exfoliated from Kish graphite. SEM, TEM and AFM images reveal the morphology of Fe_3O_4 nanoparticles. The stray field in proximity to graphene coming from each individual Fe_3O_4 nanoparticle is the primary influence on Schottky barriers of the devices, and Schottky barrier can be tuned by the quantity of Fe_3O_4 nanoparticles. This work provides a reference basis in tailoring the electrical properties of graphene by superparamagnetic Fe_3O_4 nanoparticles and paves a way to further study the magnetic transport properties of graphene decorated with Fe_3O_4 nanoparticles.

ACKNOWLEDGMENT

This work was supported by the National Key Projects for Basic Research of China (2014CB921101 and 2014CB921103), the National Natural Science Foundation of China (11274003, 61176088, and 61274102), and the Program for the New Century Excellent Talents in University (NCET-11-0240), the PAPD project, and the Fundamental Research Funds for the Central Universities.

RERFERENCES

. [1] R. A. de Groot and F. M. Mueller, "New Class of Materials: Half-Metallic Ferromagnets," Phys. Rev. Lett., vol. 50, pp. 2024-2027, 1983.

. [2] R. W. Millar, "The heat capacities at low temperatures of "Ferrous oxide," magnetite and cuprous and cupric oxides," J. Am. Chem. Soc, vol. 51, pp. 215- 222, 1929.

. [3] E. J. W. Verwey, "Electronic conduction of magnetite (Fe3O4) and its transition point at low temperatures," Nature, vol. 114, p. 327, 1939.

. [4] W.Q.Liu,P.K.J.Wong,N.J.Maltby,S.P.Li,X.F.Wang,J.Du,B.You,J. Wu, P. Bencok, and R. Zhang "Spin and orbital moments of nanoscale Fe3O4 epitaxial thin film on MgO/GaAs(100)," Appl. Phys. Lett., vol. 104, p. 142407, 2014.

. [5] H. Tian, J. Verbeeck, S. Bruck, M. Paul, D. Kufer, M. Sing, R. Claessen, and G. V. Eendeloo, "Interface-induced modulation of charge and polarization in thin film Fe3O4," Adv. Mater., vol. 26, pp. 461-5, Jan 22 2014.

. [6] S. Gálvez, J. Rubio-Zuazo, E. Salas-Colera, A. Muñoz-Noval, and G. R. Castro, "Sharp chemical interface in epitaxial Fe3O4 thin films," Appl. Phys. Lett., vol. 105, p. 241603, 2014.

. [7] D. Reisinger, P. Majewski, M. Opel, L. Alff, and R. Gross, "Hall effect, magnetization, and conductivity of Fe3O4 epitaxial thin films," Appl.Phys. Lett., vol. 85, p. 4980, 2004.

. [8] C. Wang, C. Xu, H. Zeng, and S. Sun, "Recent Progress in Syntheses and Applications of Dumbbell-like Nanoparticles," Adv. Mater., vol. 21, pp. 3045- 3052, 2009.

. [9] A. H. Castro Neto, N. M. R. Peres, K. S. Novoselov, and A. K. Geim, "The electronic properties of graphene," Rev. of Mode. Phys., vol. 81, pp. 109-162, 2009.

. [10] K. S. Novoselov, A. K. Geim, S. V. Morozov, D. Jiang, M. I. Katsnelson, I. V.

Grigorieva, S. V. Dubonos, and A. A. Firsov "Two-dimensional gas of massless Dirac fermions in graphene," Nature, vol. 438, pp. 197-200, Nov 10 2005.

. [11] M. A. H. Vozmediano, M. P. López-Sancho, T. Stauber, and F. Guinea, "Local defects and ferromagnetism in graphene layers," Phys. Rev. B, vol. 72, p, 155121, 2005.

. [12] A. A. Kozikov, D. W. Horsell, E. McCann, and V. I. Fal'ko, "Evidence for spin memory in the electron phase coherence in graphene," Phys. Rev. B, vol. 86, 2012.

. [13] W. Han, R. K. Kawakami, M. Gmitra, and J. Fabian, "Graphene spintronics," Nat. Nanotechnol, vol. 9, pp. 794-807, Oct 2014.

. [14] K. S. Novoselov, S. V. Morozov, D. Jiang, Y. Zhang, S. V. Dubonos, I. V. Grigorieva, A. A. Firsov, "Electric Field Effect in Atomically Thin Carbon Films," Science, vol. 306, p. 666, 2004.

. [15] D. Zhan, J. Yan, L. Lai, Z. Ni, L. Liu, and Z. Shen, "Engineering the electronic structure of graphene," Adv. Mater., vol. 24, pp. 4055-69, Aug 8 2012.

. [16] J. H. Conan Weeks, Jason Alicea, Marcel Franz, and Ruqian Wu, "Engineering a Robust Quantum Spin Hall State in Graphene via Adatom Deposition," Phys. Rev. X, vol. 1, p. 021001, 2011.

. [17] F. Miao, Y. Zhang, U. C. Coskun,. Bao, C. N. Lau, "Phase-Coherent Transport in Graphene Quantum Billiards," Science, vol. 317, p. 1530, 2007.

. [18] T. Gang, M. D. Yilmaz, D. Atac, S. K. Bose, E. Strambini, A. H. Velders, M. P. De Jong, J. Huskens, and W. G. van der Wiel "Tunable doping of a metal with molecular spins," Nat. Nanotechnol, vol. 7, pp. 232-6, Apr 2012.

. [19] A. H. Castro. Neto. and. F. Guinea, "Impurity-Induced Spin-Orbit Coupling in Graphene," Phys. Rev. Lett., vol. 103, p. 026804, 2009.

. [20] W. Han, K. Pi, K. M. McCreary, Y. Li, J. J. I. Wong, A. G. Swartz, and P. K. Kawakami "Tunneling Spin Injection into Single Layer Graphene," Phys. Rev. Lett., vol. 105, p. 167202, 2010.

. [21] X. Hong, K. Zou, B. Wang, S. H. Cheng, and J. Zhu, "Evidence for Spin-Flip Scattering and Local Moments in Dilute Fluorinated Graphene," Phys. Rev. Lett., vol. 108, p. 226602, 2012.

. [22] H. Jiang, Z. Qiao, H. Liu, J. Shi, and Q. Niu, "Stabilizing Topological Phases in Graphene via Random Adsorption," Phys. Rev. Lett., vol. 109, p. 116803, 2012.

. [23] C. L. Kane and E. J. Mele, "Quantum Spin Hall Effect in Graphene," Phys.Rev. Lett., vol. 95, p. 226801, 2005.

. [24] M. Lundeberg, R. Yang, J. Renard, and J. Folk, "Defect-Mediated Spin Relaxation and Dephasing in Graphene," Phys. Rev. Lett., vol. 110, p. 156601, 2013. [25] Y. Zhang, Y. W. Tan, H. L. Stormer, and P. Kim, "Experimental observation of the quantum Hall effect and Berry's phase in graphene," Nature, vol. 438, pp. 201-4, Nov 10 2005.

. [26] D. Xiao, W. Yao, and Q. Niu, "Valley-Contrasting Physics in Graphene: Magnetic Moment and Topological Transport," Phys. Rev. Lett., vol. 99, p. 236809, 2007.

. [27] H. Zhang, C. Lazo, S. Blügel, S. Heinze, and Y. Mokrousov, "Electrically Tunable Quantum Anomalous Hall Effect in Graphene Decorated by 5d Transition-Metal Adatoms," Phys. Rev. Lett., vol. 108, p. 056802, 2012.

. [28] Y. Qin, J. Han, G. Guo, Y. Du, Z. Li, Y. Song , P. Li, W. F. Wang, X. G. Wang, M. Han, and F. Q. Song, "Enhanced quantum coherence in graphene caused by Pd cluster deposition," Appl. Phys. Lett., vol. 106, p. 023108, 2015.

. [29] G. Cheng, L. Wei, L. Cheng, H. Liang, X. Zhang, H. Li, G. L. Yu, and C. G. Zeng "Graphene in proximity to magnetic insulating $LaMnO_3$," Appl. Phys. Lett., vol. 105, p.

133111, 2014.

. [30] Z. Wang, C. Tang, R. Sachs, Y. Barlas, and J. Shi, "Proximity-Induced Ferromagnetism in Graphene Revealed by the Anomalous Hall Effect," Phys. Rev. Lett., vol. 114, p. 016603, 2015.

. [31] Q.Y.An,F.Lv,Q.Q.Liu,C.H.Han,K.N.Zhao,J.Z.Sheng,Q.L.Wei,M.Y. Yan, and L. Q. Mai, "Amorphous Vanadium Oxide Matrixes Supporting Hierarchical Porous Fe3O4/Graphene Nanowires as a High-Rate Lithium Storage Anode," Nano. Lett., vol. 14, pp. 6250-6, Nov 12 2014.

. [32] D.K. Kim, W. Voit, K.V. Rao, M. Muhammed, "Synthesis and characterization of surfactant-coated superparamagnetic monodispersed iron oxide nanoparticles," J. Mag. and Mag. Mater., vol. 225, pp. 30-36, 2001.

. [33] R. R. Nair, A. N. Grigorenko, K. S. Novoselov, T. J. Booth, T. Stauber, N. M. R. Peres, A. K. Geim, "Fine Structure Constant Defines Visual Transparency of Graphene," Science, vol. 320, p. 1308, 2008.

. [34] X.-L. Tang, H.-W. Zhang, H. Su, and Z.-Y. Zhong, "A novel spin-polarized transport effect based on double-Schottky barriers," Physica E: Low- 0018-9464 (c) 2015

FIGURES

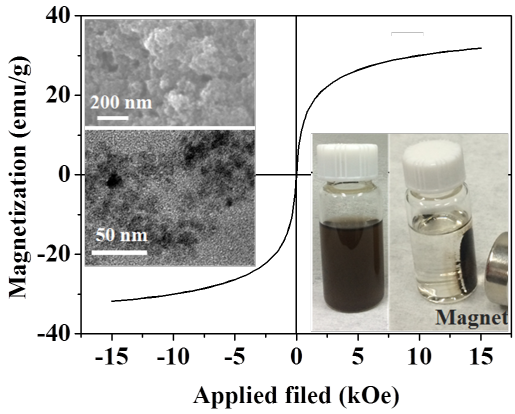

Fig. 1 Magnetic hysteresis loop of Fe3O4 nanoparticles, clearly indicating superparamagnetism of large quantity Fe3O4 nanoparticles. Experimental (black solid rectangle) and calculated (red solid line) data represent the best fit for the Langevin function. Left top and bottom insets are SEM and TEM images. Right bottom inset is photograph before and after magnet attraction, denoting ferromagnetism of each individual Fe3O4 nanoparticle.

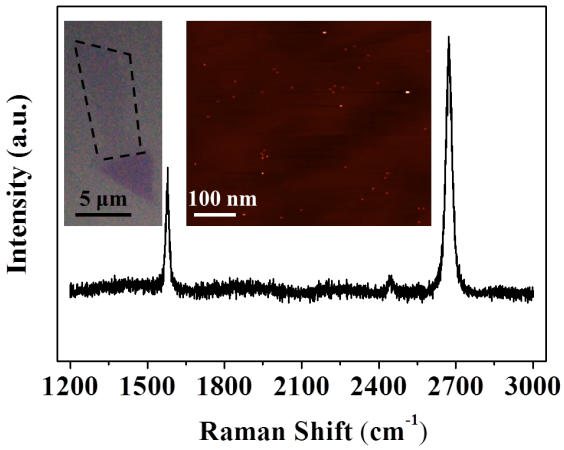

Fig. 2 Raman spectrum of typical graphene sample, the 2D peak and 2D/G ratio indicate that the sample is a single-layer graphene sheet. Left inset is optical micrograph of single-layer graphene, and the dashed lines show the edges of the single-layer graphene sheet. Right inset shows an AFM image of the graphene sheet with Fe3O4 nanoparticles. Fig.3 (a) I-V curves of S1 (black rectangle line for pure graphene) and S2 (red circle line for graphene with 0.05 ml alcohol). The left top inset shows the optical micrograph of S1. The dashed lines show the edges of the single-layer graphene sheet. The right bottom inset is the I-V curve of S1 with 0.05 ml alcohol-soluble Fe3O4 nanoparticles solution. (b) I-V curves of S3 (graphene decorated with different volumes (0, 0.05, and 0.1 ml) of alcohol-soluble Fe3O4 nanoparticles solution). Inset is I-V curves of S4 measured at the larger voltage.

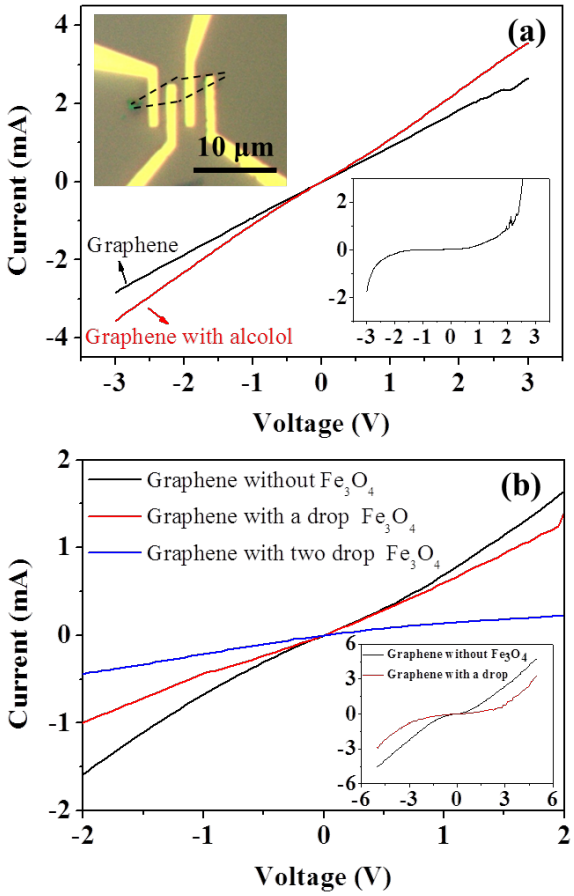

Fig.3 (a) *I-V* curves of pure graphene and graphene after dripping a drop of alcohol. The left top inset shows the optical micrograph of the device, the dashed lines show the edges of the single-layer graphene sheet. The right bottom inset is the *I-V* curve of graphene a drop of alcohol Fe_3O_4 nanoparticles solution. (b) *I-V* curves of graphene decorated with different drops of Fe_3O_4 nanoparticles solution, inset is *I-V* curves of another sample measured at larger voltage.